Physica A 502 (2018) 590–604

Contents lists available at ScienceDirect

Physica A

journal homepage: www.elsevier.com/locate/physa

Temporal correlations in the Vicsek model with vectorial noise

Damián Gulich [a,b,*], Gabriel Baglietto [a,b], Alejandro F. Rozenfeld [c,d]

[a] Instituto de Física de Líquidos y Sistemas Biológicos, CONICET, UNLP, Calle 59 Nro. 789, 1900 La Plata, Argentina
[b] Departamento de Ciencias Básicas, Facultad de Ingeniería, Universidad Nacional de La Plata (UNLP), 1900 La Plata, Argentina
[c] Núcleo INTELYMEC (Facultad de Ingeniería-UNCPBA), Argentina
[d] CIFICEN (UNCPBA-CICPBA-CONICET), Olavarría, Argentina

ARTICLE INFO

Article history:
Received 19 June 2017
Received in revised form 22 November 2017
Available online 27 February 2018

Keywords:
Vicsek model
Self-propelled particles
Scaling range
Fractality
Detrended Fluctuation Analysis
Time series analysis

ABSTRACT

We study the temporal correlations in the evolution of the order parameter $\phi(t)$ for the Vicsek model with vectorial noise by estimating its Hurst exponent H with *detrended fluctuation analysis* (DFA). We present results on this parameter as a function of noise amplitude η introduced in simulations. We also compare with well known order–disorder phase transition for that same noise range. We find that – regardless of detrending degree – H spikes at the known coexistence noise for phase transition, and that this is due to nonstationarities introduced by the transit of the system between two well defined states with lower exponents. We statistically support this claim by successfully synthesizing equivalent cases derived from a transformed fractional Brownian motion (TfBm).

1. Introduction

What we now know as the *Vicsek Model* (VM) is a metric model based on the supposition that each element (without an internal structure) in a swarm has a tendency to mimic the motion of its neighbors, being this interaction affected by an intrinsic noise [1]. Despite its inherent simplicity, the VM presents many outstanding features such as phase transitions, self-organization and fluctuations (many and varied studies based on the VM can be found on reviews [2–4] and cited references). The original VM has been studied under several theoretical approaches, being the hydrodynamics formulation by Toner and Tu [5] one of the most influential. In this context we must also cite Bialek et al. [6] for their quantitative microscopic theory to describe starlings flocking based on experimental data.

Natural systems, such as the human heart rate [7], internet traffic [8], invasion percolation [9], financial time series [10–12], or space storms [13] are known to show phase transitions related to fractal properties usually measured by Hurst exponents. Recently, Zhao et al. [14] have studied the correlations present in a second order phase transition (2D Ising) and have found that the generalized Hurst exponent can serve as an early phase transition warning. In this work we study the temporal correlations present in the order parameter time series for the Vicsek model with vectorial noise undergoing a phase transition.

The remainder of this work is organized as follows: in Section 2 we detail the Vicsek model with vectorial noise; in Section 3 we discuss the DFA framework used to analyze the order parameter time series with results presented in Section 4. In Section 4.1 we discuss the presence and relevance of nonstationarities in the series at phase transition. Finally, the conclusions are detailed in Section 5.

* Corresponding author at: Instituto de Física de Líquidos y Sistemas Biológicos, CONICET, UNLP, Calle 59 Nro. 789, 1900 La Plata, Argentina.
E-mail address: dgulich@ciop.unlp.edu.ar (D. Gulich).

https://doi.org/10.1016/j.physa.2018.02.094
0378-4371/

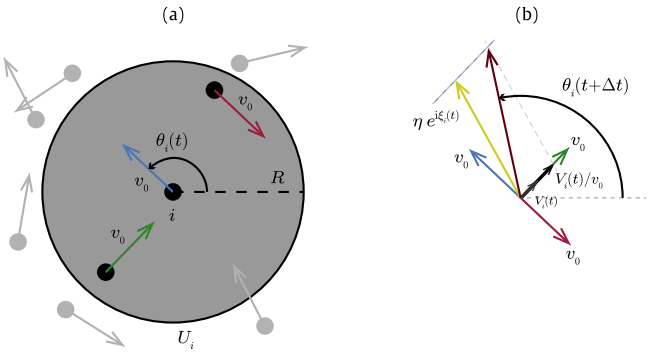

Fig. 1. The Vicsek model with vectorial noise. (a) Particles to be considered in the circular neighborhood of particle i. (b) Computation of V_i for particles in U_i and vectorial noise adding to find $\theta_i\,(t+\Delta t)$ ($v_0 = 1/2$).

2. The Vicsek model with vectorial noise (VMVN)

We simulate N particles in a two dimensional box of sides L with periodic boundary conditions (a particle leaving the box from one side re-enters on the opposite side), moving at a fixed speed v_0 [1]. Each particle has a position $\vec{r}_i\,(t)$ and a uniform speed v_0. At $t = 0$ we [we distribute the N particles across the box by assigning random initial positions and angles (the angles θ_i are in the $[-\pi, \pi]$ range). Changes in particle velocity are due to angle $\theta_i\,(t)$. Now, for a given particle we center a circular neighborhood $U_i\left(\vec{r}_i; R; t\right)$ (where R is a maximal interaction distance for all particles) and calculate the average velocity among neighbor particles:

$$\vec{V}_i\,(t) = \frac{1}{k_i\,(t)} \sum_{j:\vec{r}_j \in U_i}^{k_i(t)} \vec{v}_j\,(t) \tag{1}$$

where $k_i\,(t)$ is the total number of particles in U_i (this includes the particle itself, as it is clarified in Fig. 1-a).

The spatial evolution of the particle will be affected by a noise factor; in this work we shall use the *vectorial noise* as proposed by Chaté et al. [15]. This is how a particle's angle is updated based on the average local velocity described in Eq. (1), and how this in turn updates velocity and position:

$$\begin{aligned} \vec{r}_i\,(t+\Delta t) &= \vec{r}_i\,(t) + \vec{v}_i\,(t)\ \Delta t \\ \theta_i\,(t+\Delta t) &= \text{Angle}\left\{\vec{V}_i\,(t)\,/v_0 + \eta\, e^{\mathbf{i}\xi_i(t)}\right\} \\ \vec{v}_i\,(t+\Delta t) &= v_0\, e^{\mathbf{i}\theta_i(t+\Delta t)} \end{aligned} \tag{2}$$

where the "Angle" function is defined as $\text{Angle}\left\{u_0 e^{\mathbf{i}\theta_0}\right\} = \theta_0$ (we here use the complex number representation of 2D vectors for simplicity), $\xi_i\,(t)$ is a random number uniformly distributed in the $[-\pi; \pi]$ range, η is the noise intensity and the time increment per simulation step is $\Delta t = 1$ (Fig. 1-b). Note that the updated positions $\vec{r}_i\,(t+\Delta t)$ are based on velocities prior to update $\vec{v}_i\,(t)$ (this is known as the *backward update rule* [16]).

2.1. The order parameter

The *order parameter* [1,17] (sometimes called *general consensus*) is an instantaneous value given by the set of agents' velocities according to

$$\phi_\eta\,(t) = \frac{1}{N v_0} \left\| \sum_{i=1}^{N} \vec{v}_i \right\|. \tag{3}$$

It should be noted that $\phi_\eta\,(t)$ is also a noisy time series. Simulated systems begin with a very low order parameter in initial conditions ($\phi_\eta\,(t=0) \sim 0$, disordered phase) since all particles start with velocity v_0 in random directions and after a sufficiently long simulation time τ, the system (away from coexistence noise) will reach a unimodal order parameter distribution. In order to establish if a proposed τ is appropriate, we study the curve $\left\langle \phi_\eta\,(t) \right\rangle$ (average across realizations). As follows,

1. Divide the interval $I = [\tau; T]$ in 10 sub-intervals (being T the total simulated time).
2. Calculate the set of slopes m of a linear regression of $\left\langle \phi_\eta\,(t) \right\rangle$ in each sub-interval.
3. Find the average slope $\langle m \rangle$.

If $\langle m \rangle$ satisfies

$$\langle m \rangle \leq \frac{\sigma\,(m)}{\sqrt{10}} \tag{4}$$

(where $\sigma\,(m)$ is the standard deviation), then it may be considered that all local approximations fluctuate around a constant value ($\langle m \rangle \sim 0$) beyond that short initial transient. Having found a suitable τ we can concatenate all realizations[1] with a given noise intensity η in one set $\Phi\,(\eta) = \left\{\phi_\eta^j\,(\tau \leq t \leq T)\right\}$ and therefore the order parameter as a function of noise intensity is:

$$\phi\,(\eta) = \langle \Phi\,(\eta) \rangle \tag{5}$$

where the average is over the values of $\Phi\,(\eta)$.

Despite the fact that the VM is a far-from-equilibrium system [18], it is useful to adopt as an observable the following definition of *susceptibility* ($\chi\,(\eta)$), based on the variance of the order parameter [19]:

$$\chi\,(\eta) = \left[\left\langle \Phi^2 \right\rangle - \langle \Phi \rangle^2\right] N \tag{6}$$

where $\Phi \equiv \Phi\,(\eta)$ [20–22] (the reader may find an interpretation of this definition in Ref. [19]).

Another observable used to find critical points is the static (fourth order) Binder cumulant [15,23,24] given by

$$U\,(\eta) = 1 - \frac{\left\langle \Phi^4 \right\rangle}{3\left\langle \Phi^2 \right\rangle^2}. \tag{7}$$

3. DFA measures and adjustment criterion

3.1. DFA

In order to characterize temporal correlations present in order parameter time series $\phi\,(t)$ we will use *Detrended Fluctuation Analysis* (DFA) for the estimation of the Hurst exponent (H). Since the seminal work on DFA by Peng et al. [25] and its multifractal generalization (MF-DFA) by Kantelhardt et al. [26] this technique has been widely used in time series analysis and it is the most popular approach to detect the presence of long-term memory in data [27].

The DFA method follows five steps that we shall briefly enumerate (the reader will find a more detailed explanation in Refs. [26,28]).

- Step 1: given a time series $X = \{x_t, t = 1, \ldots, W\}$, with W being the number of equidistant observations, the cumulated data series $Y\,(k) = \sum_{t=1}^{k} (x_t - \langle x \rangle)$, with $k = 1, \ldots, W$ and $\langle x \rangle = \left(\sum_{t=1}^{W} x_t\right)/W$, is considered.
- Step 2: this profile is divided into $\lfloor W/s \rfloor$ non-overlapping windows of equal length s ($\lfloor a \rfloor$ denotes the largest integer less than or equal to a).
- Step 3: a local polynomial fit $y_{\nu,\,m}\,(k)$ of degree m is fitted to the profile for each window $\nu = 1, \ldots, \lfloor W/s \rfloor$. The degree of the polynomial can be varied to eliminate constant ($m = 0$), linear ($m = 1$), quadratic ($m = 2$) or higher order trends of the profile.
- Step 4: the variance of the detrended time series is evaluated by averaging over all data points k in each segment ν,

$$F_m^2\,(\nu, s) = (1/s) \sum_{k=1}^{s} \left\{Y\,[(\nu - 1)\,s + k] - y_{\nu,\,m}\,(k)\right\}^2$$

  for $\nu = 1, \ldots, \lfloor N/s \rfloor$.
- Step 5: the DFA fluctuation function is obtained by averaging over all segments and taking the square root,

$$F_m\,(s) = \left\{(1/\lfloor W/s \rfloor) \sum_{\nu=1}^{\lfloor W/s \rfloor} \left[F_m^2\,(\nu, s)\right]\right\}^{1/2}. \tag{8}$$

This procedure should be repeated for different values of the time scale s in order to unveil the s-dependence of F_m. If the time series has long-range power-law correlations, $F_m\,(s)$ scales as

$$F_m\,(s) \sim s^H \tag{9}$$

for a certain range of s [29]. The H exponent is estimated by the slope of the best linear regression in a double logarithmic plot[2] . The long-range correlations embedded in the time series are quantified by this exponent [30,31]:

[1] It is common practice to find a single value of τ suitable for all noise intensities and realizations.

[2] $\log \equiv \log_{10}$ in this work.

- A Hurst exponent value $0 < H < 0.5$ will exist for an *anti-persistent process* in which an increase will tend to be followed by a decrease and vice versa (negative autocorrelation).
- A value $H = 1/2$ is obtained for uncorrelated data, indicative of a true random process (a Brownian time series) in which there is no correlation between any element and a future element.
- A Hurst exponent value $0.5 < H < 1$ indicates a *persistent process* in which consecutive increments tend to have the same sign (positive autocorrelation).

It should be noted that Step 1 of this technique is due to historical reasons in the development of DFA. In the original article by Peng *et al.* [25] the raw nucleotide series analyzed were derivatives of processes whose correlations were to be studied. The way to skip this step and find the properties of the series of interest is simply to give as input to the algorithm the discrete derivative of the series to be analyzed. ($\tilde{x}_t = x_{t+1} - x_t$).

3.2. Criterion based on goodness of linear fit

Suppose x_t is a time series and we have M given scales[3] s: $s \equiv \{s_1, s_2, \ldots, s_M\}$ for which we have already calculated the fluctuation function $F_m(s) \equiv \{F_m(s_k)\}$ $(1 \leq k \leq M)$. The following algorithm introduced by Gulich et al. [29] determines the optimum scale fitting range for the fluctuation function associated to the series:

1. Define a minimum amount of data points δ. In practice, this parameter should be no less than 10 so that a linear fit makes statistical sense. Values of δ between $\lfloor M/4 \rfloor$ and $\lfloor M/3 \rfloor$ will discriminate regions of at least that amount of data points, which is a reasonable partition of the data set.
2. Prepare the data points for linear fitting: calculate the logarithmic series $L_s = \{\log(s_k)\}$ and $L_F = \{\log(F_m(s_k))\}$ $(1 \leq k \leq M)$.
3. Define a matrix $r_{M\times M}$ of default values equal to 0 in which will keep the coefficients of determination of each linear fit.
4. Compute all non-zero elements of r according to $r_{ij} = R^2(s_i, s_j)$ where $R^2(s_i, s_j)$ is the coefficient of determination (R^2) of the linear fit of L_F versus L_s between (and including) $\log(s_i)$ and $\log(s_j)$. Also $1 \leq i \leq (M - \delta + 1)$ and $(i + \delta - 1) \leq j \leq M$. By definition, every $r_{ij} \leq 1$ and non-zero values are in the diagonal superior region of the matrix.
5. Sort all non-zero values r_{ij} in decreasing order while keeping record of their original subindices.
6. If there are repeated values in r, sorting requires an extra criterion; based on length of interval choose first the longest one (in amount of data points).

The first element of this list will then provide the best linear fit interval (*'Dominant'*) and the rest will follow it in decreasing quality. Since the slope of linear fit in the range estimates the scaling exponent H (according to Eq. (9)), we have found the best estimation range for this parameter. With decreasing adjustment quality, it is also possible to find intervals to the left of the Dominant interval (*'Previous'*) or to the right (*'Next'*) intervals.

This method has proven effective in finding optimal fitting regions, which are characteristic of each time series [29]. However, in dealing with many time series (i.e. many realizations with the same noise intensity) the problem arises of deciding common fitting regions so that the results are comparable to each other. The way to overcome this problem is to draw a histogram of the scales of the edges of all detected regions regardless of their classification (Dominant, Previous, or Next). An identification of local frequency maxima then allows defining the most likely fitting regions for the entire set of fluctuation functions. If the regions determined by this method are juxtaposed, then the scales separating one region from the other can be interpreted as crossover scales.

4. Results and discussion

We simulated $N = 1024$ particles in a two dimensional box of sides $L = 32$ with periodic boundary conditions (particle density $\rho = 1$), moving at a fixed speed $v_0 = 0.5$ and an interaction radius $R = 1$. Total simulation steps were $T = 300\,000$ and instantaneous values of order parameter ϕ were recorded every 50 simulation steps (every time series of order parameters was then 6000 values long). Noise intensity η ranged from 0.1 to 0.8 and 10 realizations were simulated[4] for each noise value (changing random simulation seed). Typical configurations at time T are shown in Fig. 2 for both the ordered and disordered phases.

In Fig. 3-a we show the averaged realizations $\langle \phi_\eta(t) \rangle$. A suitable value of τ was found to be 10 000 (green line); with this value we then calculated the order parameter as a function of noise intensity $\phi(\eta)$ (Fig. 3-b), as well as Binder cumulant $U(\eta)$ (Fig. 3-c) and susceptibility $\chi(\eta)$ (Fig. 3-d). The Binder cumulant shows a maximum at $\eta = 0.609$ and the susceptibility at

[3] Equally log-spaced.

[4] Noises below 0.1 are more representative of an inelastic collision.

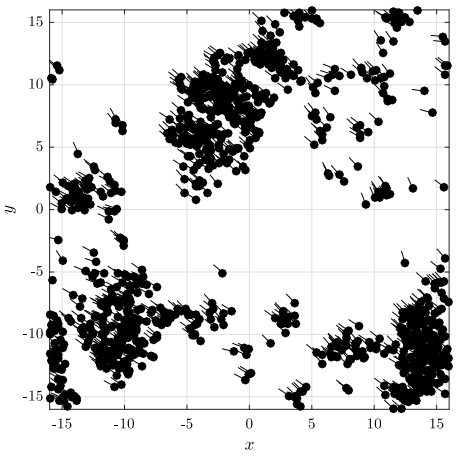

(a) $\eta = 0.1 - t = 300000$.

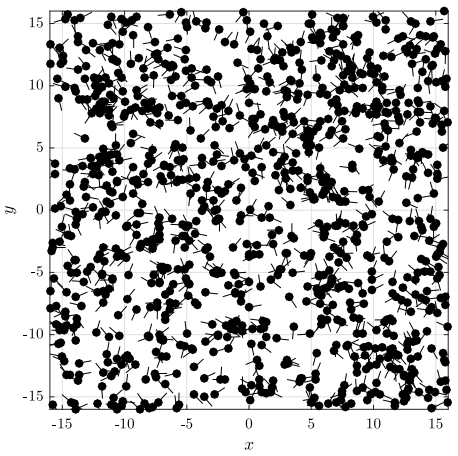

(b) $\eta = 0.8 - t = 300000$.

Fig. 2. Typical configurations at $t = 300\,000$. $N = 1024$ particles, $L = 32$ with periodic boundary conditions (particle density $\rho = 1$), speed $v_0 = 0.5$ and an interaction radius $R = 1$. (a) $\eta = 0.1$ (ordered phase). (b) $\eta = 0.8$ (disordered phase).

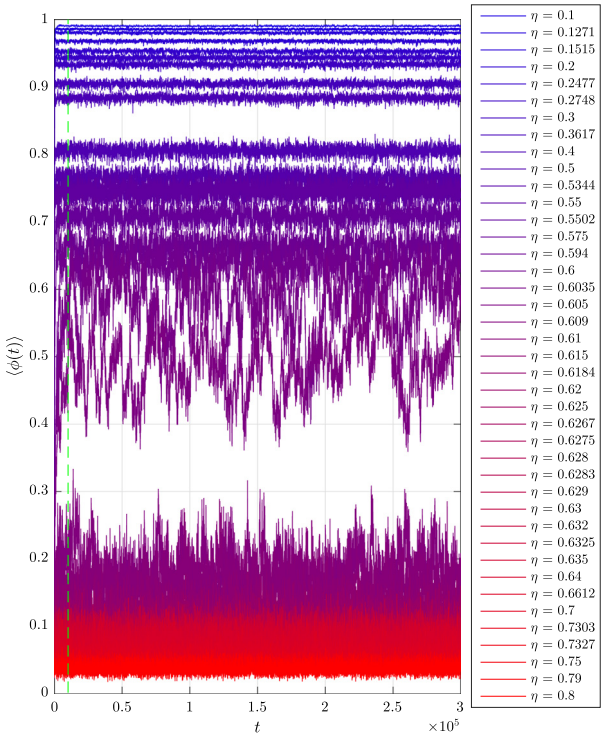

(a) Order parameter (average of 10 realizations).

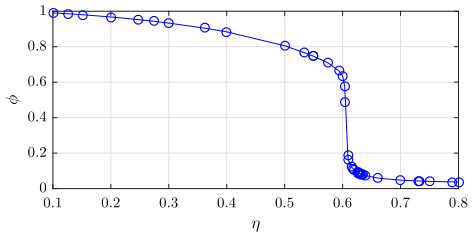

(b) Order parameter — VMVN model $\rho = 1$; $N = 1024$.

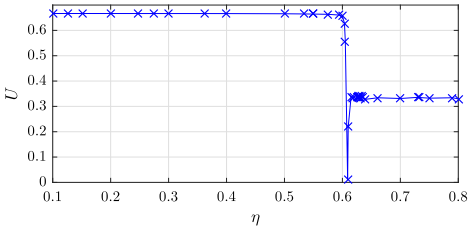

(c) Binder cumulant (on concatenated $\phi(t)$).

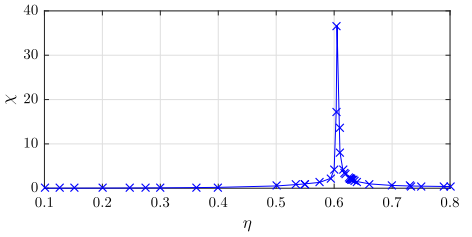

(d) Susceptibility χ, $\rho = 1$; $N = 1024$.

Fig. 3. (a) Order parameters based on noise intensity, averaged over 10 realizations. Based on this plot, the proposed τ value for the rest of the analysis was 10000 (vertical green dotted line). (b) Order parameter as a function of noise intensity $\phi(\eta)$. (c) Binder cumulant $U(\eta)$. The coexistence noise intensity from this graph is $\eta_c^U = 0.609$. (d) Susceptibility $\chi(\eta)$. The coexistence noise intensity from this graph is $\eta_c^\chi = 0.605$.

a very close value $\eta = 0.605$; critical noise $0.605 \leq \eta_c \leq 0.609$. In Fig. 4 we show the probability distribution functions of 10 concatenated order parameter realizations $\Phi(\eta) = \left\{\phi_\eta^j\,(\tau \leq t \leq T)\right\}$, which are monomodal away from coexistence value η_c. The order parameter evolution may be qualitatively regarded as under the influence of an effective potential of the

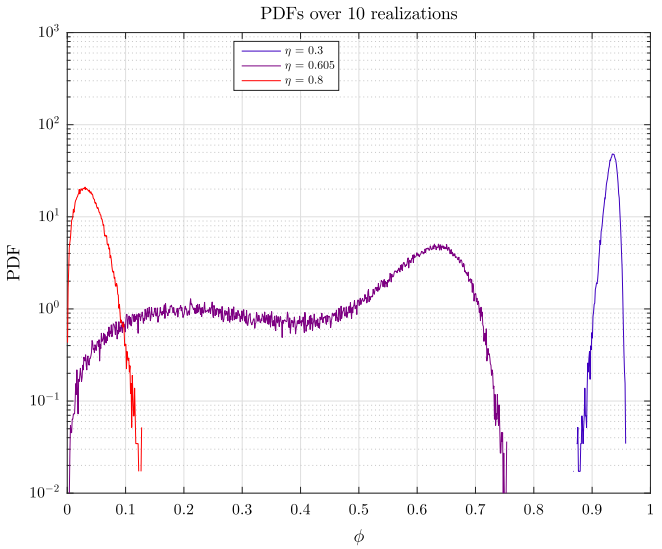

Fig. 4. Probability distribution functions of 10 concatenated order parameter realizations $\Phi(\eta) = \left\{\phi_\eta^j(\tau \leq t \leq T)\right\}, \tau = 10\,000$. The PDFs are monomodal away from phase transition ($0.605 \leq \eta_c \leq 0.609$) and bimodal close to η_c.

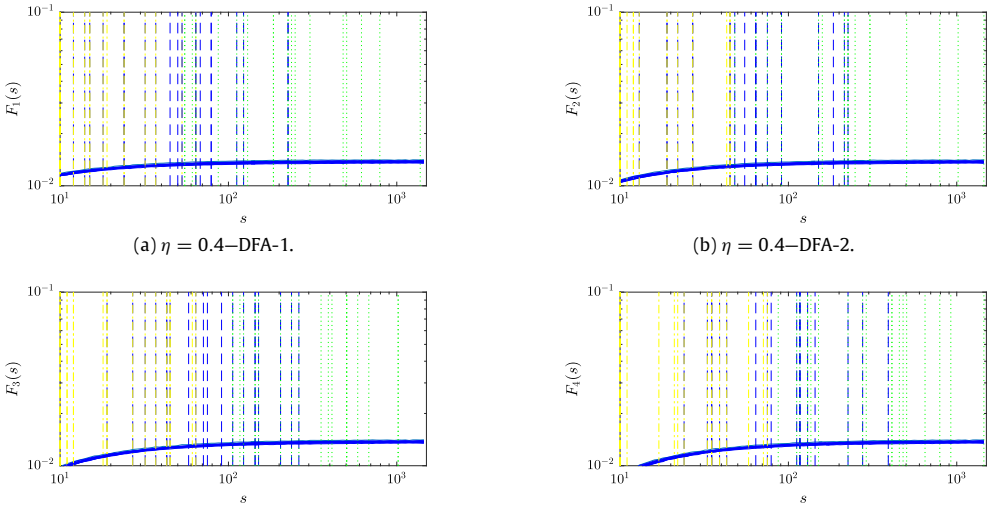

(a) $\eta = 0.4$—DFA-1. (b) $\eta = 0.4$—DFA-2.

(c) $\eta = 0.4$—DFA-3. (d) $\eta = 0.4$—DFA-4.

Fig. 5. Fluctuation functions of all 10 realizations for noise intensity $\eta = 0.4$. Vertical lines show edges of all detected optimal fitting regions ($\delta = 25$). Criterion detected edges in vertical lines: dashed blue (Dominant), dotted green (Next), dot–dash (Previous).

form $V(\phi) = -\log(\text{PDF})$ [32]. Away from phase transition these time series are stationary, while near coexistence noise stationarity is lost due to the transit between two well defined means (a source of nonstationarities in the series).

The series analyzed were discretely differentiated to be able to use the algorithm described in Section 3.1 omitting the integration step (Step 1). We performed a DFA analysis of all realizations and noise intensities with 100 scales $10 \leq s \leq 1449$; detrending degrees were $m = 1, 2, 3, 4$ [33]. For each function of fluctuation we look for the optimal fitting regions with the criterion detailed in Section 3.2 (we show this output in Fig. 5).

In order to determine fitting regions for all series, we studied the regions edges histogram for every detrending degree (from all noise intensities an all realizations). We show this result in Fig. 6, where it may be seen that local maxima at $s = 53$–65 (average $s = 59$). The two DFA fitting regions for all fluctuations will then be $S_1 = [10, 59]$ (short scales) and $S_2 = [59; 1449]$ (we shall too analyze the long scales correlations), being $s = 59$ the crossover scale.

In Fig. 7 we show the results of estimated H in regions S_1 and S_2 versus noise intensity. In both cases we find an anti-persistent process ($0 < H < 0.5$). This result is reasonable, since far from the coexistence noise the order parameter is monomodal and with low dispersion, which means that a departure of the mean in either direction is probably followed by

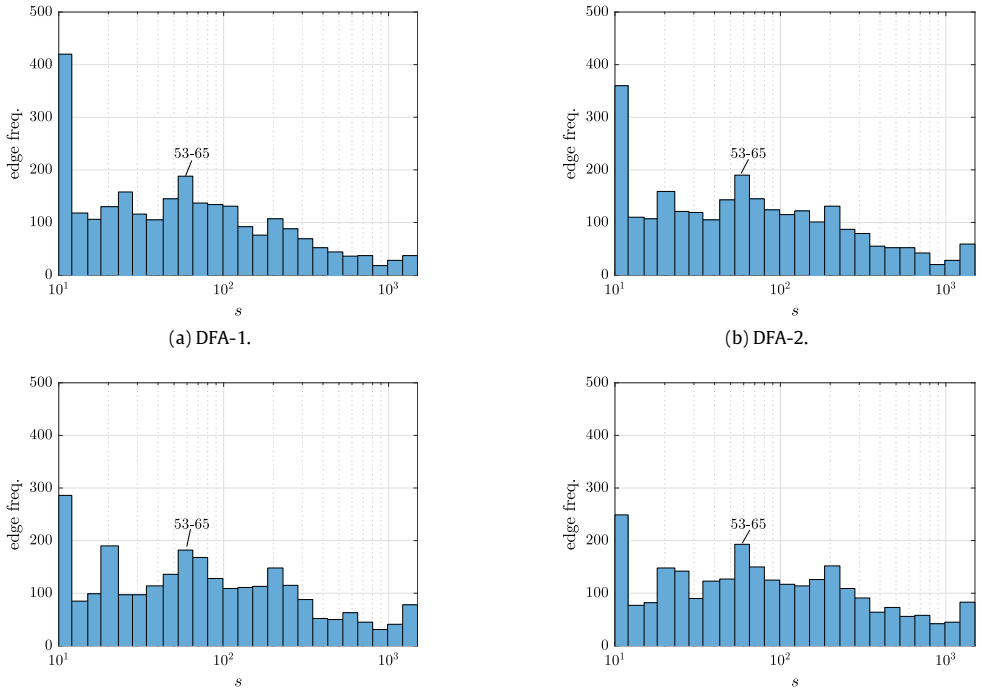

(a) DFA-1. (b) DFA-2.

(c) DFA-3. (d) DFA-4.

Fig. 6. Histograms for fitting zones edges. Every histogram resumes all edges of fitting regions for DFA found for all realizations and all noise levels. The detrending degree for subplots a–d is 1–4. In all cases there is a local maximum at $s = 53 - 65$. Therefore fitting regions for DFA will be $S_1 = [10, 59]$ and $S_2 = [59, 1449]$.

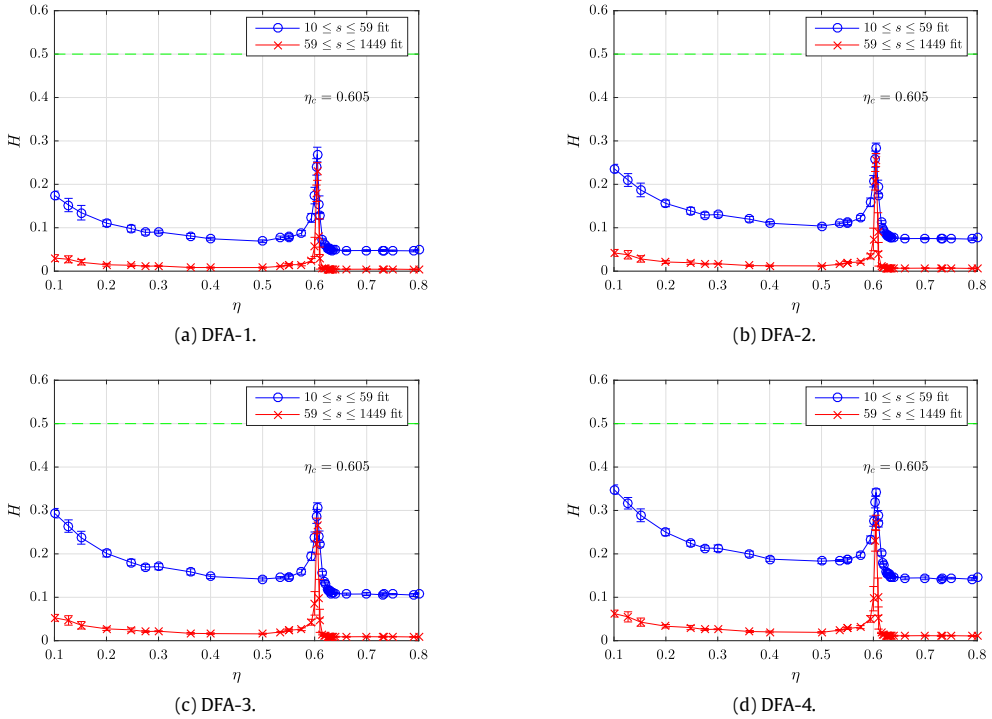

(a) DFA-1. (b) DFA-2.

(c) DFA-3. (d) DFA-4.

Fig. 7. Average H over 10 realizations versus η (error bars from std). The detrending degree for subplots a–d is 1–4. In blue circles estimations fitted in the $S_1 = [10, 59]$ interval (short scales), in red $\times$s estimations fitted in the $S_2 = [59, 1449]$ interval (long scales).

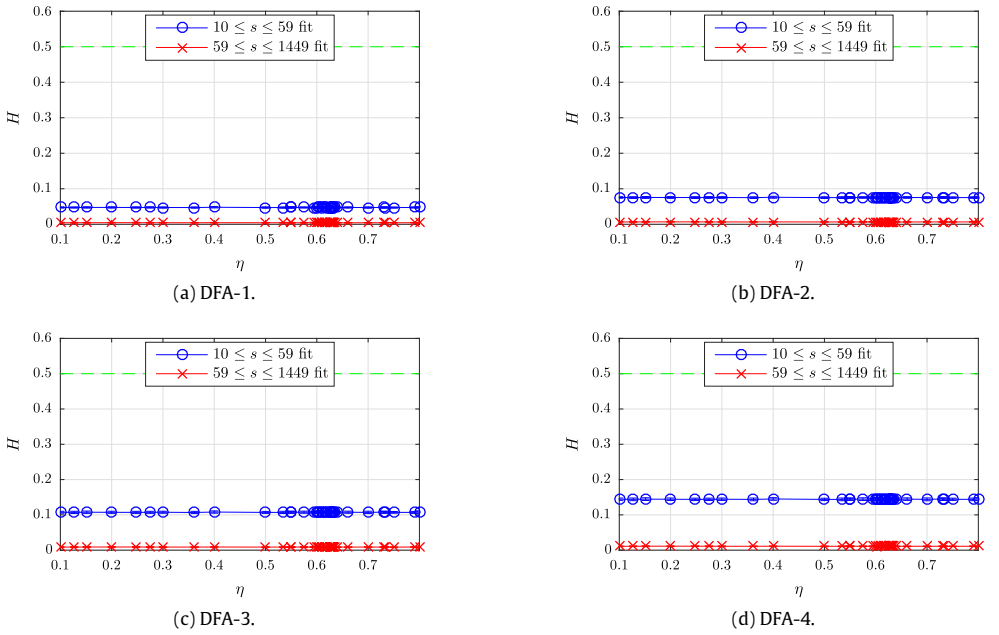

(a) DFA-1. (b) DFA-2.

(c) DFA-3. (d) DFA-4.

Fig. 8. Average H over 10 realizations and 10 random shuffles each versus η (error bars from std). The detrending degree for subplots a–d is 1–4. In blue circles estimations fitted in the $S_1 = [10, 59]$ interval (short scales), in red $\times$s estimations fitted in the $S_2 = [59, 1449]$ interval (long scales) as done in Fig. 7.

an offset in the opposite direction [34]. The very definition of $\phi_\eta(t)$ in the [0, 1] interval (Eq. (3)), the PDFs (Fig. 4) or the potentials, and the sufficient length of the obtained time series reassure this observed range of H.

The adjustment in short scales (blue circles in the figure) always produces H exponents greater than those found for long scales (red $\times$s in the figure), regardless of the detrending degree (results are stable as discussed by Oświęcimka et al. [33]). For both short and long scales, the exponent value decreases from its starting value slowly from $\eta = 0.1$ to $\eta = 0.5$; while at $\eta_c^H = 0.605$ a well-defined peak ($H \sim 0.3$) is found which then drops rapidly to a stable value (the long scales spike is always sharper than the short scales one). This general behavior is observed in all cases and so it is not due to a detrending artifact.

We performed 10 random shuffles of each of the series used and repeated the previous analysis of H as shown in Fig. 8. We find that the peaks disappear and the resulting exponents are constant, taking the value thrown by the original series for noises greater than the coexistence noise (disordered phase). This shows that, as expected, the structure of the time series plays an important role in the dynamics observed in the order parameter. However, in the next section we discuss that at coexistence noise we must also consider the role of the order parameter transit between two separate values since this is the source of nonstationarities in the considered series [35] (the shuffling process also destroys the nonstationarities present in the series near coexistence noise).

4.1. Interpretation of Hurst exponent spike at coexistence noise

To interpret the Hurst exponent peak observed in coexistence noise level, we will study the correlations characteristics present in that case. In Fig. 9-a we show a typical case of order parameter when $\eta = 0.605$. The distribution for this realization (Fig. 9-b) is consistent with that shown in Fig. 4, so that we will take the case as representative of the whole set.

In order to simplify this discussion, we will restrict the analysis in this section to DFA-2[5] with fitting in the full range of scales (an analysis with different degrees of detrending and dominant scales will give similar results). In Fig. 9-c we show the result of the DFA analysis of the order parameter series obtaining a Hurst exponent $H_c = 0.260 \pm 0.002$ (consistent with that observed in Fig. 7-b). The hypothesis we introduce is that this high exponent compared to those seen away from coexistence noise (except for very low noise) is due to the continuous transit of the order parameter between two well-defined metastable states, each with a lower Hurst exponent. As shown in Fig. 4, there are two attractive phases in which the system can be trapped depending on noise intensity. Undergoing dynamics creates consensus under low noise level. That is translated into anti-persistence in order parameters' time series towards higher values of noise intensity (close to 1). Anti-persistence is quantitatively denoted by low values of H ($H < 0.5$). However, as we approach coexistence noise value

[5] As in the previous analysis, the series are discretely differentiated before being processed by the traditional algorithm.

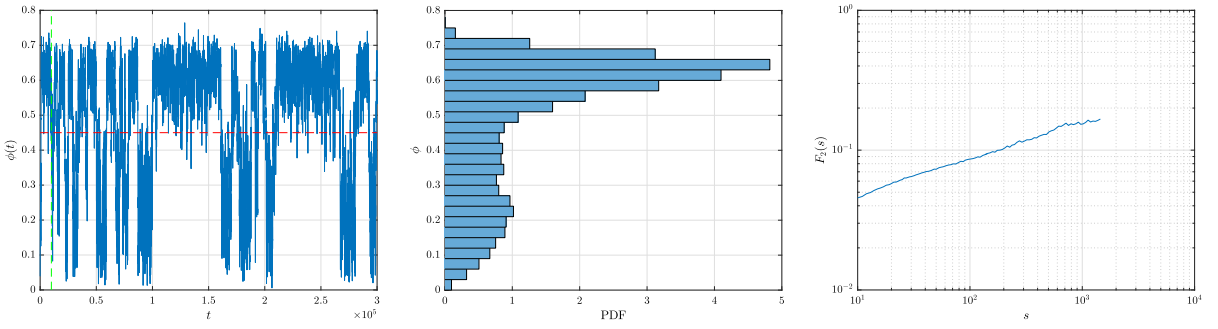

(a) Time series, $\eta = 0.605$. (b) PDF from τ. (c) Fluctuation function, $H = 0.260 \pm 0.002$ (full range fit).

(d) Separated time series, $\eta = 0.605$. (e) PDFs. (f) Fluctuation functions.

Fig. 9. Study of bimodality in order parameter time series at coexistence noise ($\eta = 0.605$). (a) Typical order parameter output for the VMVN. The green dashed vertical line indicates $\tau = 10\,000$; while the red dashed horizontal line indicates a threshold value $\phi_0 = 0.45$. (b) PDF of ϕ ($\tau \leq t \leq T$) for realization shown in -a. (c) DFA-2 fluctuation function of ϕ ($\tau \leq t \leq T$). Fitting in the full range of scales ([10, 1449]) we obtain $H_c = 0.260 \pm 0.002$. (d) Decomposition of series shown in -a ($\tau \leq t \leq T$) into two subseries: series 1 (blue, 3876 datapoints) is made with values $\phi \geq \phi_0$ and series 2 (red, 1924 datapoints) is made with values $\phi < \phi_0$. (e) PDF for both subseries: series 1 (blue, mean = 0.6078 and std = 0.0618) and series 2 (red, mean = 0.2536 and std = 0.1132). (f) DFA-2 fluctuation functions for both subseries: series 1 (blue) and series 2 (red). Fitting in the each full range of scales we obtain $H_1 = 0.111 \pm 0.004$ and $H_2 = 0.157 \pm 0.005$. (For interpretation of the references to color in this figure legend, the reader is referred to the web version of this article.)

(from below, Fig. 7) the consensus dynamic is weakened, increasing the persistence of the process (increasing H towards 0.5). Once the system transited to no-consensus phase, anti-persistent undergoing processes takes control again, considerably reducing H. Away from coexistence noise the series are stationary, while close to coexistence noise, the bimodality of the series is a source of nonstationarities.

The original order parameter series (5798 data points) can be decomposed into two subsets: one with all the original consecutive values equal or above one threshold and one analogous with values below the threshold (this is shown in Fig. 9-d where the threshold chosen is 0.45). In Fig. 9-e we show the statistical properties of both subseries: series 1 (blue, mean = 0.6078 and std = 0.0618) and series 2 (red, mean = 0.2536 and std = 0.1132). The DFA analysis of each of the subseries (Fig. 9-f) shows that it is effectively two processes with Hurst exponents smaller than the complete series from which they come: $H_1 = 0.111 \pm 0.004$ (series 1) and $H_2 = 0.157 \pm 0.005$ (series 2).

4.1.1. Synthesis of series

In order to see if previous decomposition result corresponds to a more general rule we decided to test the validity of the inverse path: given two synthetic processes with

1. similar mean and std to studied subseries,
2. Hurst exponents similar to H_1 and H_2,

combine them so that the resulting series shows an exponent compatible with H_c ($>H_1, H_2$) - a systematic study of several nonstationarities related to this technique can be found in the work of Chen et al. [35]. As a starting point, we used the MATLAB `wfbm` (H_0, L) function[6] to simulate fractional Brownian motions (fBm), with a given Hurst exponent H_0 and series length L. In order to be able to satisfy the statistical distribution requirements of the simulated data (average and std) and

[6] Following the algorithm proposed by Abry and Sellan [36].

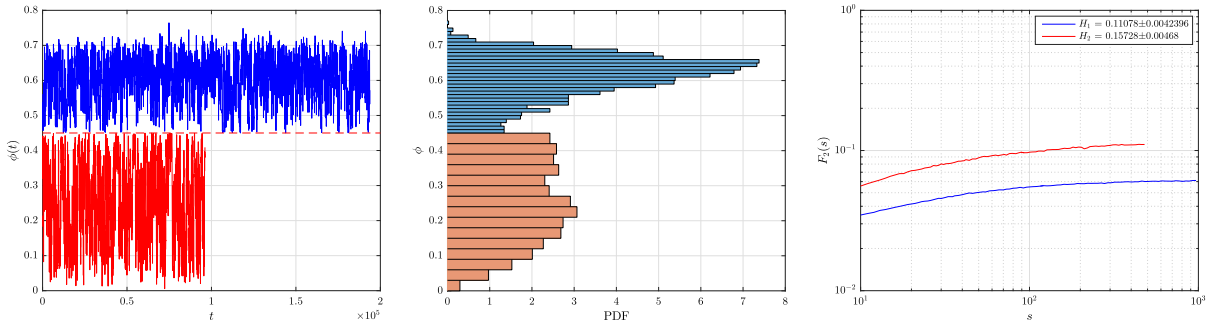

(a) Generated TfBms. (b) PDFs. (c) Fluctuation functions.

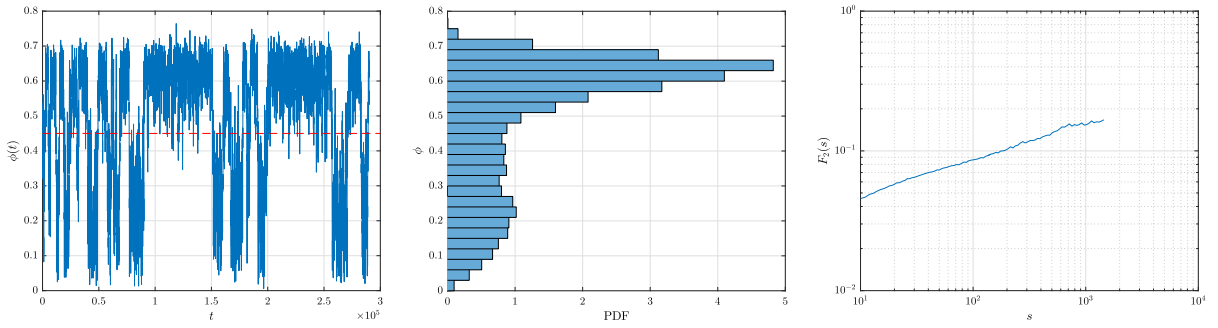

(d) Concatenated TfBms. (e) PDF. (f) Fluctuation function, $H = 0.273 \pm 0.001$ (full range fit).

Fig. 10. Transformed fractional Brownian motion reconstruction of $\phi\,(t)$ at coexistence noise (Fig. 9). (a) Transformed fBms subseries (TfBm); TfBm series 1 (blue, 3875 data points) and TfBm series 2 (red, 1923 data points). The red dashed horizontal line indicates a threshold value $\phi_0 = 0.45$. (b) PDF for both subseries: TfBm series 1 (blue, mean = 0.6078 and std = 0.0618) and TfBm series 2 (red, mean = 0.2536 and std = 0.1132). (c) DFA-2 fluctuation functions for both subseries: TfBm series 1 (blue) and TfBm series 2 (red). Fitting in the each full range of scales we obtain $H_1 = 0.113 \pm 0.002$ and $H_2 = 0.143 \pm 0.003$. (d) Both subseries concatenated after being split in 15 random length blocks (a block from series 1 is followed by a block of 2 and so on). the red dashed horizontal line indicates the threshold value. (e) PDF of the full synthesized series (-d). This distribution is in good agreement with the original simulated series (Fig. 9-b). (f) DFA-2 fluctuation function of the fractional Brownian motion reconstruction. Fitting in the full range of scales ([10, 1449]) we obtain $H = 0.273 \pm 0.001$. (For interpretation of the references to color in this figure legend, the reader is referred to the web version of this article.)

Hurst exponents (after discrete differentiation), we followed a trial and error process and found that appropriate generation conditions are:

$$\begin{aligned} \texttt{series1} &= \texttt{wfbm}(0.02, 3875) \\ \texttt{series2} &= \texttt{wfbm}(0.10999, 1923) \end{aligned} \tag{10}$$

while the transformation of statistical distribution features gives the desired *transformed fractional Brownian motion* (TfBm):

$$\begin{aligned} \texttt{TfBm series1} &= 0.6078 + (0.0618/\texttt{std}\,(\texttt{series1})) \cdot \texttt{series1} \\ \texttt{TfBm series2} &= 0.2536 + (0.1132/\texttt{std}\,(\texttt{series2})) \cdot \texttt{series2}. \end{aligned} \tag{11}$$

Both TfBm series are shown in Fig. 10-a, and their statistical distributions are depicted in Fig. 10-b. The DFA result (full range fit) is shown in Fig. 10-c; TfBm series 1 (blue, $H_1 = 0.113 \pm 0.002$) and TfBm series 2 (red, $H_2 = 0.143 \pm 0.003$). The above shows that both generated TfBms satisfy conditions 1 and 2, and it remains to detail the method of mixing the two series. For this purpose, we will simply divide each TfBm into 15 random length blocks[7] and concatenate them starting with block 1 of TfBm series 1 followed by block 1 of TfBm series 2, then block 2 of TfBm series 1 followed by block 2 of TfBm series 2 and so on (the result of this concatenation is shown in Fig. 10-d). The PDF of the concatenated series (Fig. 10-d) is in good agreement with that of the original series (Fig. 9-b), while the Hurst exponent calculated (full range fit) for this series is $H = 0.273 \pm 0.001$ (Fig. 10-f), which is also approximately the same as that observed for the original series ($H_c = 0.260 \pm 0.002$, Fig. 9-c).

[7] This number was chosen based on the amount of larger blocks in the series, however the following results remain valid for a considerable amount of blocks as seen in Fig. 11.

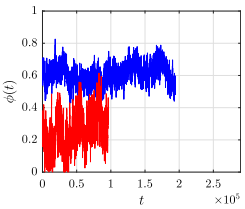

(a) Generated TfBms.

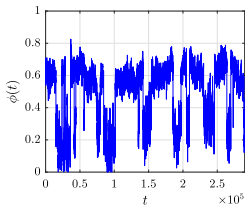

(b) Concatenated TfBms, 15 blocks.

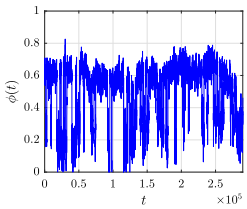

(c) Concatenated TfBms, 50 blocks.

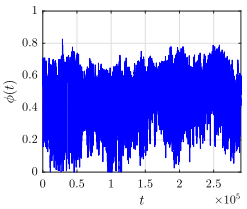

(d) Concatenated TfBms, 500 blocks.

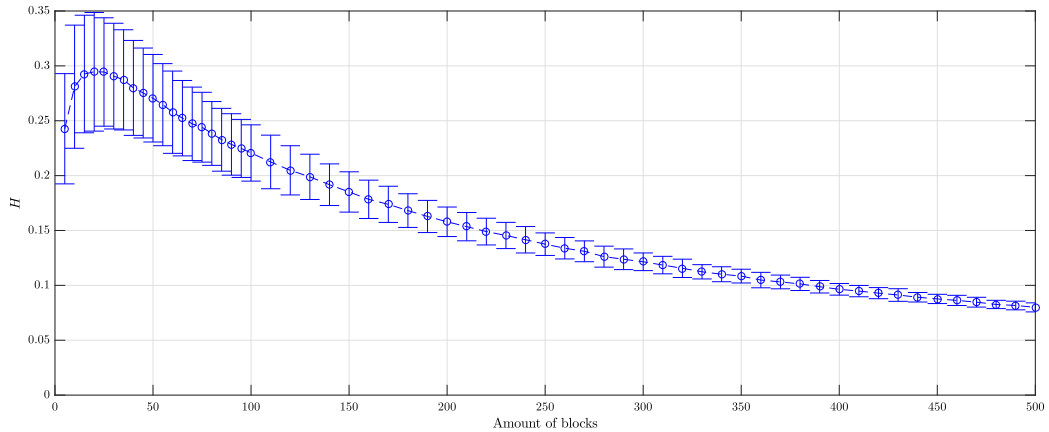

(e) H of concatenated TfBms (DFA-2)—full range fit.

Fig. 11. (a) Transformed fractional Brownian motion subseries as in Fig. 10. (b–d) Reconstruction of $\phi(t)$ at coexistence noise with subseries from -a concatenating 15, 50 and 500 blocks respectively. (e) Average H over 100 realizations (error bars from std) versus the amount of concatenated blocks (DFA-2, full range fit).

Table 1
Summary of results.

	mean	std	H
Representative series	–	-	0.260 ± 0.002
Concatenated series (100 ensemble)	–	-	0.28 ± 0.06
Series 1 (representative series)	0.6078	0.0618	0.111 ± 0.004
TfBm series 1 (100 ensemble)	0.6078	0.0618	0.106 ± 0.007
Series 2 (representative series)	0.2536	0.1132	0.157 ± 0.005
TfBm series 2 (100 ensemble)	0.2536	0.1132	0.16 ± 0.01

To give more statistical support to this result we have repeated this process of synthesis with the same characteristics detailed in 100 independent cases. The averages for the generated TfBms were $H_1 = 0.106 \pm 0.007$ and $H_2 = 0.16 \pm 0.01$, while for the concatenated series we find $H = 0.28 \pm 0.06$ (all errors are the corresponding stds). These results are summarized in Table 1.

To investigate the impact on concatenated series exponent due to the amount of time a synthesized system spends in a given state, we generate TfBms as in the previous paragraph, but varying the number of blocks used (Fig. 11). We find that under these conditions there is a definite maximum of H between the 15–25 blocks ($H \sim 0.3$, Fig. 11-e); considering error bars this maximum remains to over 100 blocks. Up to 180 blocks, the Hurst exponent of the concatenated series is larger than the largest exponent of the subseries ($H_2 = 0.16$), while using over then 380 blocks the exponent is less than the smallest of the exponents of the two subseries ($H_1 = 0.11$). Note that the uncertainty in H also decreases with the number of blocks.

We have carried out an ensemble analysis of block sizes and found that for blocks with higher order parameter sizes were up to approximately $s = 80$, while for lower order parameters sizes were up to approximately $s = 30$. The average between these two widths is close the one indicated as a cutoff scale ($s = 59$).

4.1.2. The effect of threshold value

In Fig. 12 we show the effect of the threshold value ϕ_0 on the values of H for each of the subseries as detailed above (in this case we averaged over 20 realizations at coexistence noise). At $\phi_0 = 0.1$ most of the original H information is in subseries 1, while for $\phi_0 = 0.7$ most of the information is in subseries 2. At threshold value $\phi_0 = 0.4177$ both subseries present the

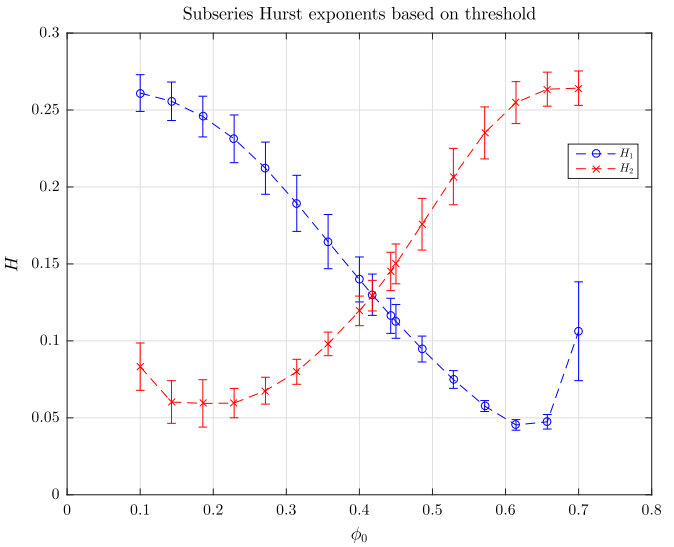

Fig. 12. H versus threshold for both obtained subseries (DFA-2, full range fit). Each point is an average of 20 realizations at coexistence noise ($\eta = 0.605$), error bars from std. Note that at $\phi_0 = 0.7$ subseries 1 values become highly dispersed due to short length of the subseries.

same Hurst exponent ($H \sim 0.13$), and we can use this extreme case to make a second and simpler argument in favor of the importance of jumps between states.

It could be argued that the effect of concatenating segments of two series with slightly different characteristics as shown above has a destructive influence on the structure of the subseries. However, the previous synthesis process respects the amount of data and the relative order of the blocks. To show the effect of jumps between states we generated 100 TfBms according to

$$\texttt{series} = \texttt{wfbm}(0.079, 6000)$$

$$\texttt{TfBm series} = 0.25359 + (0.0875/\texttt{std}\,(\texttt{series})) \cdot \texttt{series} \tag{12}$$

(this is similar to what is proposed by Chen et al. [35], sec. 4). In Fig. 13 we show a representative case in which we created an appropriate displacement function in order to create a bimodality as from simulations with just one base TfBm. The ensemble average (DFA-2, full range fit) for the TfBms is $H = 0.14 \pm 0.0017$ while the displaced ensemble average is $H = 0.309 \pm 0.0034$, again compatible with our observations.

The offset functions are step-type and cannot be analyzed by the traditional DFA methodology. Alternatively, we study to the power spectrum of the Fourier transform of the offset function (discretely differentiated) as $1/f^{\beta}$ process where $H_\beta = (\beta + 1)/2$ [31]. As a complementary analysis and to simplify the discussion, in Fig. 14 we sketch an equivalence curve between H_β And H of DFA-2 based on processes fBm with known exponents. Given a threshold value ϕ_0, it is also possible to study the original series from the point of view of displacements of a single base series (this interpretation is a simplification that does not consider the width of each of the distributions). In Fig. 14-b we take the ensemble of simulated data at coexistence noise and apply the threshold to generate a profile that flattens the series to the lowest mean (based on PDF information from Fig. 4). The opposite of this profile is an offset function just as the ones discussed above. Near $\phi_0 \sim 0.4$ wee see that, in this context, this offset is the main source of nonstationarities that increase the H value of the flattened series to the observed range of the unfiltered data (this is also in accordance with the threshold value for the previous two subseries method). This result is robust in front of ϕ_0 in a wide range around $\phi_0 \sim 0.4$ as it may be seen in Fig. 14.

In order to take a more detailed look at the structure of the offset functions found, we finally propose an adjustment based on a two-state Markov process. We generated offset functions defined by persistence probabilities p_1 for state 1 and p_2 for state 2 (this automatically sets in $1 - p_1$ the transition probability from state 1 to state 2 and $1 - p_2$ the transition probability from state 2 to state 1). We add this offset to base functions as described in Eq. (12) and compare the resulting Hurst exponent with the result from original simulated data (green line in Fig. 14). In Fig. 15 we show the resulting H as a function of parameters p_1 and p_2.

Any offset generated at the points within the red zone in Fig. 15 is satisfactory in principle to reproduce the Hurst exponent of the simulated data. However, final state-distributions must be also taken into account. In Fig. 16 we show the distributions for various combinations of p_1 and p_2 within the compatible zone. In this figure we find the combination $p_1 \sim 0.96$ and $p_2 \sim 0.98$ to be the most compatible with the original data, and therefore in this context the jumps between states can in principle be regarded as a Markov process with those approximate values. To refine the statistics, we performed 50 more realizations with those fixed parameters and found $H = 0.26 \pm 0.015$, again in agreement with our results.

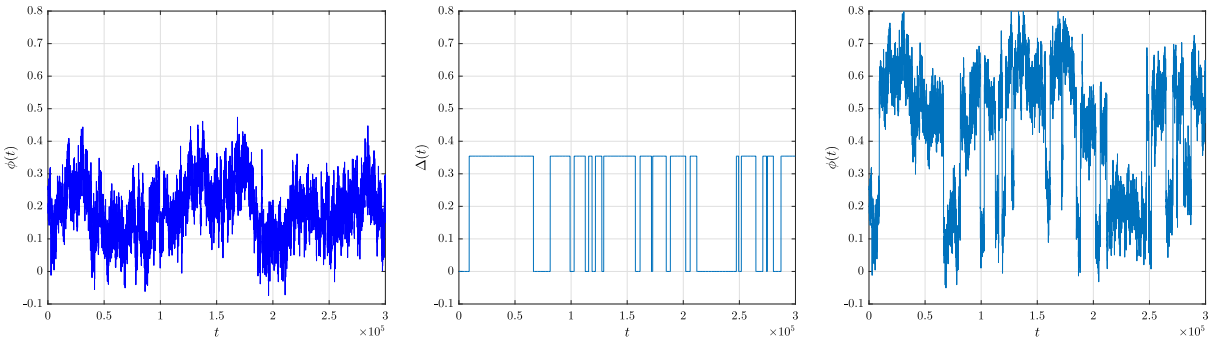

(a) Base TfBm, $H = 0.13911 \pm 0.0016876$. (b) Displacement. (c) Displaced series, $H = 0.30894 \pm 0.0033894$.

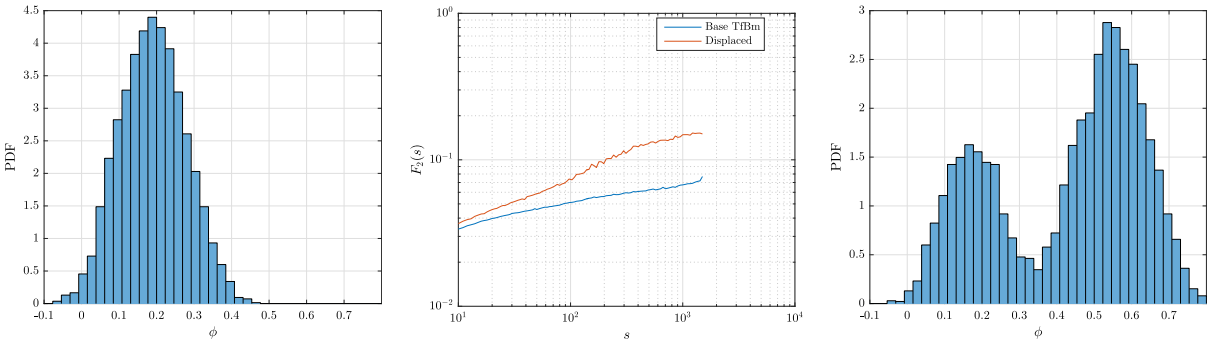

(d) PDF of base TfBm. (e) DFA-2 Fluctuations. (f) PDF of displaced series.

Fig. 13. (a) and (d) Base TfBm and its distribution ($H = 0.139 \pm 0.0017$, DFA-2, full range fit). (b) Displacement (offset) function for TfBm in (a). (c) and (f) Displaced series and its distribution ($H = 0.309 \pm 0.0034$, DFA-2, full range fit). (e) Fluctuation functions (DFA-2) for base TfBm and displaced series.

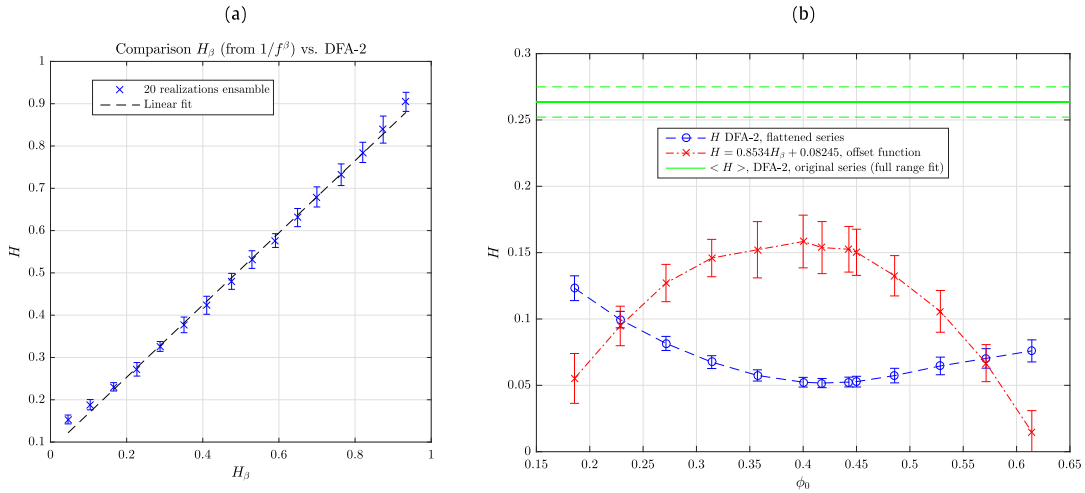

Fig. 14. (a) Simple equivalence curve between H_β (considering the series as a $1/f^\beta$ process) and H from DFA-2 (both full range fits). We generated an ensemble of 20 fBms with known H and 6000 points in length. Linear fit for equivalence is $H = 0.8537\, H_\beta + 0.08245$. (b) Simulations data: offset functions equivalent H as $1/f^\beta$ process versus ϕ_0 (red); resulting flattened series H (blue — DFA-2, full range fit); original series (green — DFA-2, full range fit). Average and std from 20 realizations.

5. Conclusions

We have used DFA to study time series taken from the dynamics of the order parameter for the VMVN with different intensities of noise. We identified a crossover scale ($s \sim 59$) in the fluctuation functions by separating short and long scales behavior. Hurst exponents for short scales (more affected by noise) are always greater than those for long scales. Throughout

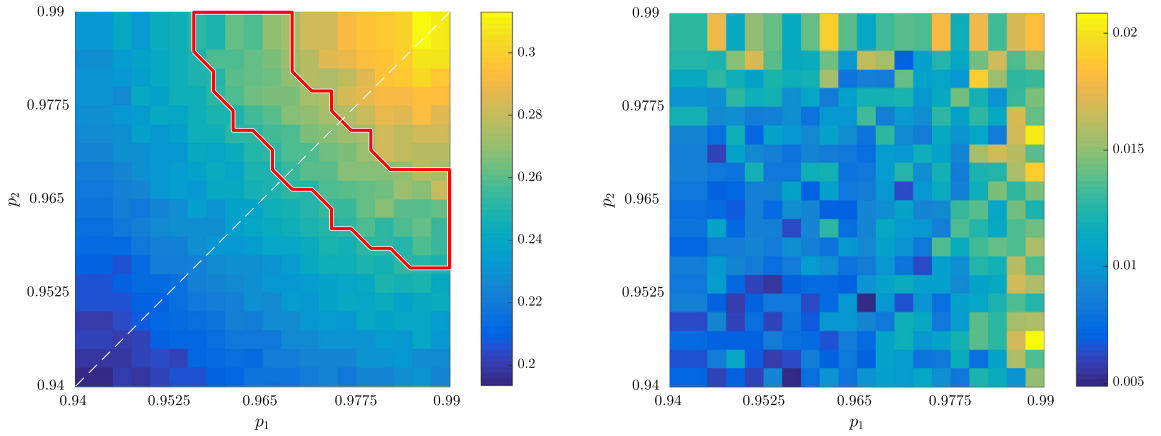

(a) H, DFA-2 full range fit, average over 20 realizations. (b) ΔH from std.

Fig. 15. Two-state model and estimation of equivalent H, ensemble over 20 realizations (6000 points each series, full range DFA-2 fit). (a) Average H; identity in white dashed line; in red we show the zone of H in the 0.2635 ± 0.0114 range (original simulated series H, see Fig. 14). (b) Error ΔH from std.

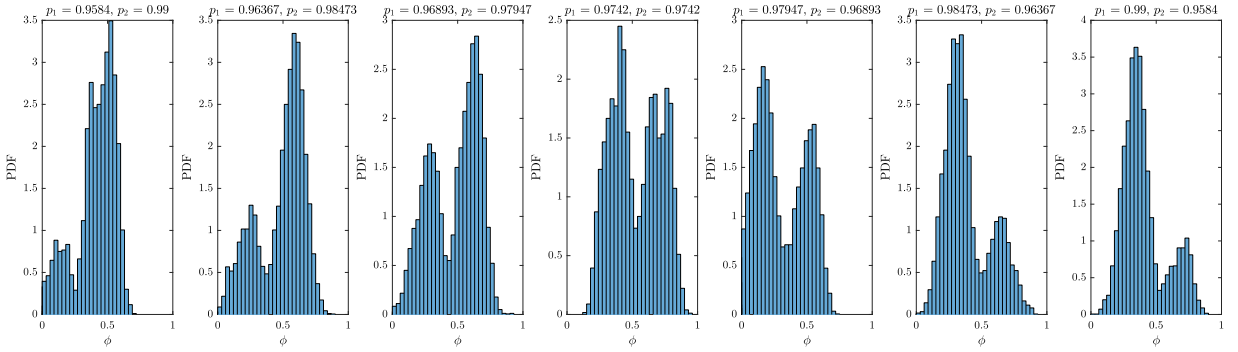

Fig. 16. Probability distribution functions of artificial series for several combinations of parameters p_1 and p_2 within the final $H \sim 0.26$ range (see Fig. 15).

the range of studied noise, the Hurst exponents show an anti-persistent process ($0 < H < 0.5$), which is expected for monomodal series, as it is the case for studied systems away from coexistence noise.

For both short scales and long scales we find a peak at $\eta_c = 0.605$ (the known phase transition noise). This peak is well defined, with a value of H greater than that observed away from η_c. Considering that the order parameter series shows a bimodal distribution near coexistence noise, we postulated that this is due to a continuous transit of the order parameter between two well-defined monomodal states, leading to nonstationarities in the series at coexistence noise. We proposed two interpretations for the study of such nonstationarities. The first considered a concatenation of two series each with a lower H exponent. We also developed a methodology to characterize and reproduce the statistical and fractal properties of order parameter series in coexistence noise using synthetic series (TfBm). We have presented a statistical argument to validate that (in these particular conditions) the proposed concatenation of two low H monomodal series leads to a higher Hurst exponent, compatible with VMVN data. In the second case we consider a base series locally displaced by offset functions. We have systematically studied the characteristics of these functions both in synthetic series and from our original simulations. In this sense, we found that it is possible to interpret the offset functions as a Markov process.

In a recent article, Zhao et al. [14] studied a peak of correlations as an indicator of the phase transition in the 2D Ising model. While at zero field the Ising model suffers a second order phase transition with a corresponding divergence of the correlation time; the Vicsek model with vectorial noise studied in the present article presents a well established first order phase transition which naturally, does not exhibit a divergence in correlation times, but, on the other hand, shows phase coexistence and metastability. Metastability introduces nonstationarities[8] in time series of the order parameter, that greatly contribute to the peak observed in H. It is well known that trends notably affect the estimation of the real correlation nature related to the intrinsic fluctuations of a series [37]; DFA and MF-DFA allow an elimination of polynomial trends of different order [38]. However, oscillatory trends (e.g. seasonal cycles [31]) are known to strongly disturb the correlation analysis and

8 In the sense of time series analysis.

are usually given a special treatment [39,40]. We conclude that in a system with a phase transition (such as the one in the VMVN) the oscillation of the order parameter near η_c may be *a priori* regarded as a handicap for DFA, but, on the contrary, opens the possibility of finding coexistence noise levels by studying the resulting spike of the Hurst exponent.

Acknowledgments

Damián Gulich, Gabriel Baglietto and Alejandro Rozenfeld were supported by Consejo Nacional de Investigaciones Científicas y Técnicas (CONICET), Argentina. Authors acknowledge financial support from CONICET PIP 11220150100039CO.

The authors thank Ezequiel V. Albano for his helpful comments on the preparation of this article.

References

[1] Tamás Vicsek, András Czirók, Eshel Ben-Jacob, Inon Cohen, Ofer Shochet, Novel type of phase transition in a system of self-driven particles, Phys. Rev. Lett. 75 (6) (1995) 1226–1229.
[2] M.C. Marchetti, J.F. Joanny, S. Ramaswamy, T.B. Liverpool, J. Prost, Madan Rao, R. Aditi Simha, Hydrodynamics of soft active matter, Rev. Modern Phys. 85 (3) (2013) 1143–1189.
[3] Tamás Vicsek, Anna Zafeiris, Collective motion, Phys. Rep. 517 (3–4) (2012) 71–140.
[4] Andreas M. Menzel, Tuned, driven, and active soft matter, Phys. Rep. 554 (2015) 1–45.
[5] John Toner, Yuhai Tu, Long-range order in a two-dimensional dynamical XY model: How birds fly together, Phys. Rev. Lett. 75 (23) (1995) 4326–4329.
[6] W. Bialek, A. Cavagna, I. Giardina, T. Mora, E. Silvestri, M. Viale, A.M. Walczak, Statistical mechanics for natural flocks of birds, Proc. Natl. Acad. Sci. 109 (13) (2012) 4786–4791.
[7] Ken Kiyono, Zbigniew R. Struzik, Naoko Aoyagi, Fumiharu Togo, Yoshiharu Yamamoto, Phase transition in a healthy human heart rate, Phys. Rev. Lett. 95 (5) (2005) 058101.
[8] Ricard V. Solé, Sergi Valverde, Information transfer and phase transitions in a model of internet traffic, Physica A 289 (3–4) (2001) 595–605.
[9] Mark A. Knackstedt, Muhammad Sahimi, Adrian P. Sheppard, Invasion percolation with long-range correlations: First-order phase transition and nonuniversal scaling properties, Phys. Rev. E 61 (5) (2000) 4920–4934.
[10] Dariusz Grech, Grzegorz Pamuła, The local Hurst exponent of the financial time series in the vicinity of crashes on the Polish stock exchange market, Physica A 387 (16–17) (2008) 4299–4308.
[11] Łukasz Czarnecki, Dariusz Grech, Grzegorz Pamuła, Comparison study of global and local approaches describing critical phenomena on the Polish stock exchange market, Physica A 387 (27) (2008) 6801–6811.
[12] Ł. Czarnecki, D. Grech, Multifractal Dynamics of Stock Markets, Acta Phys. Pol. A 117 (4) (2010) 623–629.
[13] J.A. Wanliss, P. Dobias, Space storm as a phase transition, J. Atmos. Sol.-Terr. Phys. 69 (6) (2007) 675–684.
[14] Longfeng Zhao, Wei Li, Chunbin Yang, Jihui Han, Zhu Su, Yijiang Zou, Multifractality and network analysis of phase transition, PLoS One 12 (1) (2017) e0170467.
[15] Guillaume Grégoire, Hugues Chaté, Onset of collective and cohesive motion, Phys. Rev. Lett. 92 (2) (2004).
[16] Gabriel Baglietto, Ezequiel V. Albano, Julián Candia, Complex network structure of flocks in the standard vicsek model, J. Stat. Phys. 153 (2) (2013) 270–288.
[17] Jaime A. Pimentel, Maximino Aldana, Cristián Huepe, Hernán Larralde, Intrinsic and extrinsic noise effects on phase transitions of network models with applications to swarming systems, Phys. Rev. E 77 (6) (2008).
[18] David P. Landau, Kurt Binder, A Guide to Monte Carlo Simulations in Statistical Physics, Cambridge University Press, 2009.
[19] Gabriel Baglietto, Ezequiel V. Albano, Finite-size scaling analysis and dynamic study of the critical behavior of a model for the collective displacement of self-driven individuals, Phys. Rev. E 78 (2) (2008).
[20] Ezequiel V. Albano, Gustavo Saracco, Dynamic behavior of anisotropic nonequilibrium driving lattice gases, Phys. Rev. Lett. 88 (14) (2002).
[21] S.W. Sides, P.A. Rikvold, M.A. Novotny, Kinetic ising model in an oscillating field: Finite-size scaling at the dynamic phase transition, Phys. Rev. Lett. 81 (4) (1998) 834–837.
[22] V. Manías, J. Candia, E.V. Albano, Corner wetting in a far-from-equilibrium magnetic growth model, Eur. Phys. J. B 47 (4) (2005) 563–570.
[23] K. Binder, Finite size scaling analysis of Ising model block distribution functions, Z. Phys. B: Condens. Matter 43 (2) (1981) 119–140.
[24] B. Fierro, F. Bachmann, E.E. Vogel, Phase transition in 2D and 3D Ising model by time-series analysis, Physica B 384 (1–2) (2006) 215–217.
[25] C.-K. Peng, S.V. Buldyrev, S. Havlin, M. Simons, H.E. Stanley, A.L. Goldberger, Mosaic organization of DNA nucleotides, Phys. Rev. E 49 (2) (1994) 1685–1689.
[26] Jan W. Kantelhardt, Stephan A. Zschiegner, Eva Koscielny-Bunde, Shlomo Havlin, Armin Bunde, H. Eugene Stanley, Multifractal detrended fluctuation analysis of nonstationary time series, Physica A 316 (1–4) (2002) 87–114.
[27] Dariusz Grech, Zygmunt Mazur, On the scaling ranges of detrended fluctuation analysis for long-term memory correlated short series of data, Physica A 392 (10) (2013) 2384–2397.
[28] Jan W. Kantelhardt, Eva Koscielny-Bunde, Henio H.A Rego, Shlomo Havlin, Armin Bunde, Detecting long-range correlations with detrended fluctuation analysis, Physica A 295 (3–4) (2001) 441–454.
[29] Damián Gulich, Luciano Zunino, A criterion for the determination of optimal scaling ranges in DFA and MF-DFA, Physica A 397 (2014) 17–30.
[30] Jens Feder, Fractals, Springer Nature, 1988.
[31] Eva Koscielny-Bunde, Jan W. Kantelhardt, Peter Braun, Armin Bunde, Shlomo Havlin, Long-term persistence and multifractality of river runoff records: Detrended fluctuation studies, J. Hydrol. 322 (1–4) (2006) 120–137.
[32] Miguel A. Muñoz, Romualdo Pastor-Satorras, Stochastic theory of synchronization transitions in extended systems, Phys. Rev. Lett. 90 (20) (2003).
[33] P. Oświęcimka, S. Drożdż, J. Kwapień, A.Z. Górski, Effect of detrending on multifractal characteristics, Acta Phys. Polon. A 123 (3) (2013) 597–603.
[34] Damián Gulich, Temporal correlations imaging fixed targets through turbulence, Opt. Lett. 41 (12) (2016) 2855.
[35] Zhi Chen, Plamen Ch. Ivanov, Kun Hu, H. Eugene Stanley, Effect of nonstationarities on detrended fluctuation analysis, Phys. Rev. E 65 (4) (2002).
[36] Patrice Abry, Fabrice Sellan, The wavelet-based synthesis for fractional brownian motion proposed by F. Sellan and Y. Meyer: Remarks and fast implementation, Appl. Comput. Harmon. Anal. 3 (4) (1996) 377–383.
[37] Kun Hu, Plamen Ch. Ivanov, Zhi Chen, Pedro Carpena, H. Eugene Stanley, Effect of trends on detrended fluctuation analysis, Phys. Rev. E 64 (1) (2001) 011114 (19 pages).
[38] Amir Bashan, Ronny Bartsch, Jan W. Kantelhardt, Shlomo Havlin, Comparison of detrending methods for fluctuation analysis, Physica A 387 (21) (2008) 5080–5090.
[39] R. Nagarajan, R.G. Kavasseri, Minimizing the effect of sinusoidal trends in detrended fluctuation analysis, Int. J. Bifurcation Chaos 15 (5) (2005) 1767–1773.
[40] Josef Ludescher, Mikhail I. Bogachev, Jan W. Kantelhardt, Aicko Y. Schumann, Armin Bunde, On spurious and corrupted multifractality: The effects of additive noise, short-term memory and periodic trends, Physica A 390 (13) (2011) 2480–2490.